Polymer Chemistry

Effects of tacticity and chiral center-to-dipole distance on mesogen-free liquid crystalline self-assembly of sulfonyl-containing comb-like polymers

Journal:	*Polymer Chemistry*
Manuscript ID	PY-ART-02-2020-000199.R1
Article Type:	Paper
Date Submitted by the Author:	23-Mar-2020
Complete List of Authors:	Bohannon, Caleb; The University of Tennessee, Department of Chemistry Kwok, Man-Hin; Case Western Reserve University, Macromolecular Science and Engineering Li, Ruipeng; Brookhaven National Laboratory, National Synchrotron Light Source II Zhu, Lei; Case Western Reserve University, Macromolecular Science and Engineering Zhao, Bin; The University of Tennessee, Department of Chemistry

Effects of tacticity and chiral center-to-dipole distance on mesogen-free liquid crystalline self-assembly of sulfonyl-containing comb-like polymers

Caleb A. Bohannon,[a,#] Man-Hin Kwok,[b,#,*] Ruipeng Li,[c] Lei Zhu,[b] Bin Zhao[a,*]

[a] *Department of Chemistry, University of Tennessee, Knoxville, Tennessee 37996, United States*

[b] *Department of Macromolecular Science and Engineering and Department of Chemistry, Case Western Reserve University, Cleveland, Ohio 44106-7202, United States*

[c] *National Synchrotron Light Source II, Brookhaven National Laboratory, Upton, New York 11973, United States*

[#] These authors contributed equally to this work.

* Corresponding authors. E-mail addresses: mxk977@case.edu (M.-H. Kwok) and bzhao@utk.edu (B. Zhao)

Abstract

In this report, new approaches were implemented to seek for novel ferroelectric liquid crystalline self-assembly in mesogen-free comb-like isotactic polyoxypropylenes (iPOPs) bearing mono- or di-sulfonyl groups, which have potential to exhibit high spontaneous polarization for applications in advanced electronic devices. iPOPs with *n*-alkylsulfonylpentylthioether side chains (iPOP-$SC_5SO_2C_n$, where C_n is the alkyl tail with *n* being either 12 or 8) were prepared via a post-polymerization substitution reaction from isotactic poly[(*R*)-(-)-epichlorohydrin]. The effects of main-chain tacticity, chiral center-to-dipole distance, number of sulfonyl dipoles per side chain, and *n*-alkyl tail length on the liquid crystalline self-assembly behavior were investigated by comparing iPOPs with the atactic counterparts. First, when the sulfonyl dipole was placed far away from the chiral center in iPOP-$SC_5SO_2C_n$ compared with our previously reported isotactic polyethers with *n*-alkylsulfonyl side chains (iPOP-SO_2C_n), the dipole-dipole interactions among the side chains were decreased, which led to more liquid crystalline phases. Smectic E (SmE) and A (SmA) phases were observed after the crystal melting; however, the main-chain chiral center was found to have an insignificant effect on the liquid crystalline assembly when compared to the atactic samples. Second, the longer C_n tails increased the transition temperatures as a result of stronger van der Waals interactions. Third, after the thioether linkage in the side chain was oxidized into the sulfonyl group, the chiral center-dipole and dipole-dipole interactions in the resultant polymers (i.e., iPOP-$SO_2C_5SO_2C_n$) were enhanced. As a result, the liquid crystalline phase transitions (i.e., crystal→SmE→SmA→I) were pushed to higher temperatures. The knowledge obtained in this study will help us further design and achieve the ferroelectric smectic C* phase in mesogen-free comb-like sulfonylated liquid crystalline polymers.

Keywords: Mesogen-free, comb-like polymers, chirality effect, sulfonyl dipole, polyoxypropylenes

Introduction

Ferroelectric liquid crystals[1] and liquid crystalline polymers[2] with high spontaneous polarization (P_s) are attractive functional materials for various electrical and optical applications.[3-9] However, their P_s values are usually below 10 mC/m^2, significantly lower than those of ferroelectric polymers [e.g., ~180 mC/m^2 for the β-form poly(vinylidene fluoride) (PVDF)][10,11] and ceramics (e.g., ~260 mC/m^2 for $BaTiO_3$ single crystals).[12] This can be largely attributed to the weakly dipolar groups in the molecules and bulky aromatic mesogen groups, which decrease the dipole density. The lower P_s values have prevented ferroelectric liquid crystalline polymers from being used for advanced electrical applications.

From our previous report,[13] it is desirable to realize mesogen-free liquid crystalline polymers in order to increase the dipole density. Meanwhile, highly dipolar groups, such as sulfonyl (4.5 Debye or D), cyano (3.7 D), and amide (3.9 D) groups, can be used to further increase the orientational polarization.[14] However, genuine mesogen-free liquid crystalline polymers are rather rare. Note that the rotator phases in *n*-alkanes,[15] the high pressure hexagonal phase in polyethylene[16] and isotactic poly(4-methyl-1-pentene),[17] and the paraelectric (i.e., pseudohexagonal) phase in PVDF (at high pressures)[18] and P(VDF-*co*-trifluoroethylene) [P(VDF-TrFE)][19-21] should not be considered as liquid crystalline self-assembly, because they exhibit obvious supercooling in differential scanning calorimetry (DSC) heating and cooling cycles. Therefore, it is more accurate to define them as mesophases, which are highly defective crystalline phases. One effective way to induce liquid crystalline self-assembly for aliphatic polymers is to introduce hydrogen-bonding or strong dipole-dipole interactions. For example, when L-lysine is used to link *n*-alkyl side groups to a polymethacrylate backbone, smectic liquid crystalline phases are induced with high isotropization temperature (T_i).[22,23] Later, main-chain

type poly(ester-amide)s with regular sequences also exhibit liquid crystalline self-assembly above the crystal melting temperature (T_m).[24] Replacing the amide groups with ester groups, liquid crystalline self-assembly disappears. Clearly, hydrogen-bonding plays an important role in achieving liquid crystalline self-assembly in these side-chain and main-chain amide-containing polymers.

Alternatively, sulfonyl groups are also used to induce smectic liquid crystalline phases through the incorporation in either the main chain[25-28] or side chains.[29-37] It is considered that the strong dipole-dipole interactions among the regularly distributed sulfonyl groups provide certain conformation rigidity in the soft aliphatic matrix for the mesophase assembly. For the side chain polymers, disulfonyl side groups exhibited much stronger dipole-dipole interactions than monosulfonyl groups, pushing the isotropization temperature to higher values. Regardless of different chain architectures (main chain vs. side chain) and chemical compositions (aliphatic spacer and tail lengths), only smectic A (SmA) structure was exclusively reported so far for these mesogen-free aliphatic liquid crystalline polymers. For the side-chain polymers grafted with the alkylsulfonyl groups, the regular 2_1 helical conformation is the main reason for the formation of SmA self-assembly.[13]

To achieve the ferroelectric smectic C* (SmC*) phase in mesogen-free aliphatic liquid crystalline polymers, it is necessary to induce the smectic C (SmC) phase with tilted *n*-alkyl side chains and break the C_{2h} symmetry to the C_2 symmetry by introducing chiral centers in either the main chain or the side chains.[2, 38] In the first attempt,[13] we synthesized a chiral polymer, isotactic polyepichlorohydrin (iPECH), by ring-opening polymerization of (*R*)-(-)-epichlorohydrin, and used it to prepare isotactic poly(propylene oxide) (iPOP) polymers grafted with *n*-alkylsulfonyl pendant groups (iPOP-SO_2C_n, where C_n is the *n*-alkyl tail) via post-

polymerization modifications. Although the grafting and oxidation of thioether side chains were quantitative, again only smectic A phases were obtained for samples with n = 10-12 during cooling from the isotropic melts before crystallization. Upon heating, monotropic phase behavior was observed with only crystal-melting. Therefore, new strategies need to be implemented to achieve the SmC* phase.

In this work, we first increased the distance between the chiral center in the iPOP backbone and the sulfonyl dipole in the side chain to weaken the dipole-dipole interactions and induce smectic phases through the use of *n*-alkylsulfonylpentylthioether pendant groups (Scheme 1). Subsequent oxidation of the thioether moieties led to disulfonylated iPOPs with a shorter distance between the chiral center and the inner sulfonyl group, a higher dipole density, and stronger dipole-dipole interactions. Their liquid crystalline self-assembly behaviors were thoroughly investigated by DSC, synchrotron X-ray diffraction (XRD), as well as polarized light microscopy (PLM), to examine if the ferroelectric SmC* phase could be induced via the above strategies. Atactic polyoxypropylene (aPOP) samples with sulfonylated side chains were used to compare with the iPOPs in order to study the tacticity effect on the liquid crystalline self-assembly.

Scheme 1. Syntheses of Isotactic and Atactic Polyethers with Thioether-Monosulfonyl and Disulfonyl Pendant Groups

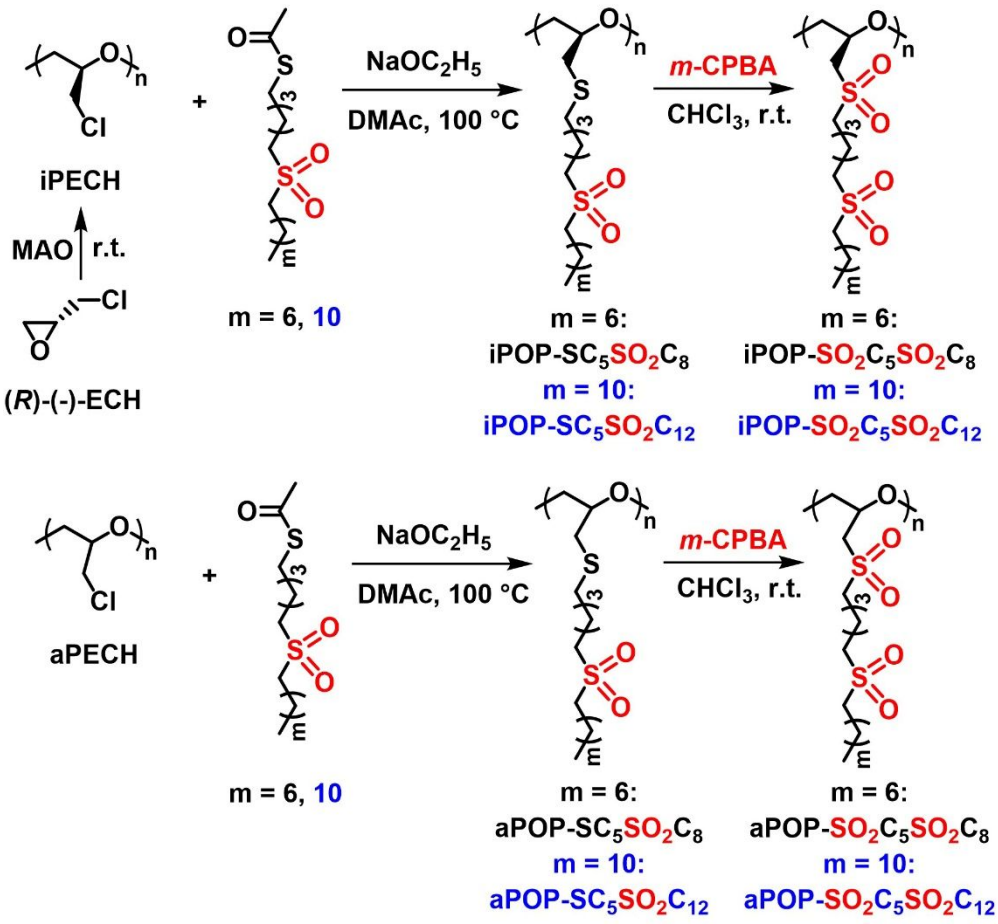

Experimental section

Materials

1-Octanethiol (97%, Acros), 1-dodecanethiol (99%, Acros), 5-bromo-1-pentanol (90%, TCI), 3-chloroperoxybenzoic acid (*m*-CPBA, 70-75% balance 3-chlorobenzoic acid and water, Acros Organics), methanesulfonyl chloride (98%, Alfa Aesar), thioacetic acid (97% Acros Organics), and *N,N*-dimethylacetamide (99.5%, extra dry, Acros Organics) were used as received. Atactic polyepichlorohydrin (aPECH) with a weight-average molecular weight (M_w) of ~700,000 Da (reported by the vendor) was obtained from Sigma-Aldrich. (*R*)-(-)-Epichlorohydrin [(*R*)-(-)-ECH, 98%, Combi-blocks, Inc.] and diethyl ether (99.8%, certified ACS, Fisher Chemical) were dried with calcium hydride (93%, Acros Organics) and distilled before use. Modified

methylaluminoxane (MMAO-12, 7 wt.% aluminum in toluene) was purchased from Sigma-Aldrich and stored in the freezer inside a nitrogen glovebox. iPECH was synthesized by ring-opening polymerization using MMAO-12 as catalyst in a glove box at room temperature as reported previously.[13] Solutions of sodium ethoxide in ethanol with concentrations of 11.3 and 13.1 wt.% were prepared by adding a calculated amount of sodium metal into absolute ethanol under a nitrogen atmosphere and stirring the mixtures until the sodium metal completely reacted. 5-(Octylsulfonyl)pentyl ethanethioate and 5-(dodecylsulfonyl)pentyl ethanethioate (Scheme 1) were synthesized according to a method reported in the literature,[34] and their molecular structures were verified by proton (^{1}H) and carbon-13 (^{13}C) NMR, and mass spectroscopy. The detailed synthesis and the characterization data are included in Section I of the Supporting Information. All other chemicals and solvents were obtained from either Fisher Scientific or Sigma-Aldrich and used as received.

Characterization and instrumentation

^{1}H and ^{13}C NMR spectra were recorded on either a Varian Mercury 300 NMR, a Varian VNMRS 500 NMR, or a Varian VNMRS 600 spectrometer using the residual solvent proton signal as the internal standard. The high-resolution mass spectrometry (HRMS) experiments were performed using a JEOL Model JMS-T100LC (AccuTOF) orthogonal time-of-flight (TOF) mass spectrometer (Peabody, MA) with an IonSense (Danvers, MA) DART source. Size exclusion chromatography (SEC) of atactic and isotactic polyethers with *n*-alkylsulfonylthioether or disulfonyl pendant groups was performed on a PL-GPC 20 system, an integrated SEC system from Polymer Laboratories, Inc., equipped with a Knauer K-2301 refractive index detector, one PL gel 5 μm guard column (50 × 7.5 mm), and two PLgel 5 μm mixed-C columns (each 300 ×

7.5 mm, linear molecular weight range of 200-2,000,000 Da). HPLC-grade chloroform was used as the eluent, and the flow rate was set at 1.0 mL/min. The SEC system was calibrated with narrow dispersity polystyrene (PS) standards (Scientific Polymer Products, Inc.), and the data was processed using the Cirrus SEC software from Polymer Laboratories, Inc.

The optical activities of isotactic polyethers with *n*-alkylsulfonylthioether pendant groups were measured at ambient temperature (~20 °C) using a PerkinElmer 241 polarimeter with a sodium lamp with a wavelength of 589 nm and an integration time of 5 s. The solutions used in the measurements were prepared by dissolving the polymers in $CHCl_3$ at a concentration of ~ 10 mg/mL. For each solution, three measurements were taken, and the average value was used as the optical rotation. The specific rotations of the polymers were calculated by using equation $[\alpha]_{\lambda}^{T} = \alpha/(cl)$, where [α] is the specific rotation at a certain temperature (T) and wavelength (λ), α is the optical rotation in degrees from the measurements, c is the concentration in units of g/mL, and l is the path length in dm. The units of specific rotation is $deg \cdot mL/(g \cdot dm)$, which is commonly abbreviated to degrees (°).

Thermogravimetric analysis (TGA) experiments were carried out in a dry nitrogen atmosphere at a heating rate of 20 °C/min from room temperature to 700 °C using TA Instruments Q-50 TGA. DSC experiments were carried out on a TA Discovery DSC 250. Approximately 3 mg samples were used at a scanning rate of 20 °C/min. PLM was carried out on an Olympus BX60, equipped with an Instec HCS402 hot stage (Instec, Inc., Boulder, CO).

Synchrotron XRD was carried out at the 11-BM Complex Materials Scattering (CMS) beamline of National Synchrotron Light Source II (NSLS-II), Brookhaven National Laboratory (BNL). The monochromatized X-ray wavelength was λ = 0.0918 nm. An in-vacuum Pilatus 800K detector (Dectris, Baden-Dättwil, Switzerland) was used for data collection. The sample-

to-detector distance was 373 mm, which was calibrated using silver behenate with the first-order reflection at a scattering vector q = 1.076 nm^{-1} [$q = (4\pi \sin\theta)/\lambda$ with θ being the half-scattering angle]. The data acquisition time was 30 s. A Linkam HFSX350 hot stage was used for temperature control. One-dimensional (1D) XRD curves were obtained by integration of the corresponding two-dimensional (2D) patterns.

Synthesis of atactic polyethers with *n*-alkylsulfonylpentylthioether pendant groups (aPOP-$SC_5SO_2C_8$ and aPOP-$SC_5SO_2C_{12}$)

aPOP-$SC_5SO_2C_8$ and aPOP-$SC_5SO_2C_{12}$ were synthesized by reacting aPECH with 5-(octylsulfonyl)pentyl ethanethioate and 5-dodecylsulfonyl)pentyl ethanethioate, respectively (Scheme 1). Shown below is the synthesis of aPOP-$SC_5SO_2C_8$. A similar procedure was used for the synthesis of aPOP-$SC_5SO_2C_{12}$. Sodium ethoxide (0.181 g, 2.65 mmol, delivered from a stock solution of sodium ethoxide in ethanol with a concentration of 13.1 wt.%) and 5-(octylsulfonyl)pentyl ethanethioate (0.822 g, 2.65 mmol) were added into a 50 mL two-necked round bottom flask with a magnetic stir bar. The mixture was stirred at room temperature for 3 h. aPECH (0.144 g, 1.56 mmol) and *N,N*-dimethylacetamide (DMAc, extra dry, 10 mL) were weighed into a 20 mL scintillation vial, which was capped, placed on a platform shaker, and shaken overnight. A clear, highly viscous solution was obtained and added into the flask containing the stirring solution of 5-(octylsulfonyl)pentyl ethanethioate and sodium ethoxide. The reaction flask was equipped with a reflux condenser, placed in an oil bath with a preset temperature of 100 ℃, and stirred for 48 h. The solution stayed clear throughout the reaction. After cooling to room temperature, the reaction mixture was precipitated in water, and the solid was collected via vacuum filtration. The polymer was then dissolved in chloroform (5 mL) and

precipitated in methanol. This dissolution-precipitation process was repeated one more time, and the collected purified polymer was dried in a vacuum oven, yielding a white fluffy solid (0.521 g, 93% yield). ^{1}H NMR (600 MHz, $CDCl_3$) δ (ppm) = 3.75 – 3.53 (m, -OCH_2CH-, 3H), 2.99 – 2.92 (m, -CH_2C$H_2$$SO_2CH_2$$CH_2$-, 4H), 2.80 – 2.51 (m, -CHCH_2SC$H_2$$CH_2$-, 4H), 1.88 – 1.77 (m, -C$H_2$$CH_2$$SO_2$$CH_2CH_2$-, 4H), 1.68 – 1.51 (m, -$CHCH_2SCH_2CH_2CH_2CH_2CH_2SO_2$-, 4H), 1.47 – 1.39 (m, -C$H_2$$(CH_2)_4CH_3$, 2H), 1.39 – 1.23 (-$CH_2$(C$H_2$)$_4$$CH_3$, 8H), 0.88 (t, -C$H_3$, 3H). ^{13}C NMR (151 MHz, $CDCl_3$), δ (ppm) = 79.20, 71.10, 70.90, 70.45, 70.25, 54.34, 52.37, 33.88, 32.65, 31.62, 29.13, 28.99, 28.87, 28.45, 27.61, 22.50, 21.79, 21.40, 13.98. SEC analysis results with chloroform as the eluent: number-average molecular weight ($M_{n,SEC}$) = 129 kDa and dispersity (*Đ*) = 3.0, relative to PS standards.

The yield for the synthesis of aPOP-$SC_5SO_2C_{12}$ was 93%. ^{1}H NMR (600 MHz, $CDCl_3$), δ (ppm) = 3.76 – 3.49 (m, ,-OCH_2CH-, 3H), 3.00 – 2.92 (m, -CH_2C$H_2$$SO_2CH_2$$CH_2$-, 4H), 2.80 – 2.52 (-CHCH_2SC$H_2$$CH_2$-, 4H), 1.89 – 1.77 (m, -C$H_2$$CH_2$$SO_2$$CH_2CH_2$-, 4H), 1.68 – 1.50 (m, -$SCH_2CH_2CH_2(CH_2)_2SO_2CH_2$-, 4H), 1.47 – 1.20 (m, -CH_2(CH_2)$_9$$CH_3$, 16H), 0.88 (t, -$CH_2CH_3$, 3H). ^{13}C NMR (151 MHz, $CDCl_3$), δ (ppm) = 79.33, 71.06, 70.94, 70.43, 70.20, 52.84, 52.39, 33.69, 32.61, 31.81, 29.53, 29.47, 29.27, 29.25, 29.17, 29.14, 29.09, 28.50, 27.62, 22.59, 21.79, 21.39, 14.03. SEC results with chloroform as eluent: $M_{n,SEC}$ = 48.3 kDa and *Đ* = 2.05, relative to PS standards.

Synthesis of isotactic polyethers with *n*-alkylsulfonylpentylthioether pendant groups (iPOP-$SC_5SO_2C_8$ and iPOP-$SC_5SO_2C_{12}$)

iPOP-$SC_5SO_2C_8$ and iPOP-$SC_5SO_2C_{12}$ were prepared from iPECH using corresponding *n*-alkylsulfonylpentyl ethanethioates via a procedure similar to that for aPOP-$SC_5SO_2C_8$ and aPOP-

$SC_5SO_2C_{12}$ (Scheme 1). The yield for the synthesis of iPOP-$SC_5SO_2C_8$: 86%. ^{1}H NMR (600 MHz, $CDCl_3$), δ (ppm) = 3.74 – 3.53 (m, -OC*H*$_2$C*H*-, 3H), 2.99 – 2.91 (m, -C*H*$_2$SO$_2$C*H*$_2$-, 4H), 2.77 –2.52 (m, -C*H*$_2$SC*H*$_2$-, 4H), 1.89 – 1.77 (m, -C*H*$_2$CH$_2$SO$_2$CH$_2$C*H*$_2$-, 4H), 1.67 – 1.52 (m, -SCH$_2$(C*H*$_2$)$_2$CH$_2$-, 4H), 1.47 – 1.39 (m, -C*H*$_2$(CH$_2$)$_4$CH$_3$, 2H), 1.36 – 1.22 (m, -CH$_2$(C*H*$_2$)$_4$CH$_3$-, 8H), 0.88 (t, -C*H*$_3$, 3H). ^{13}C NMR (151 MHz, $CDCl_3$), δ (ppm) = 80.04, 72.13, 52.84, 52.39, 33.90, 33.12, 31.63, 29.15, 29.00, 28.89, 28.47, 27.63, 22.51, 21.80, 21.41, 14.00. SEC results with chloroform as eluent: $M_{n,SEC}$ = 92.4 kDa and $Đ$ = 2.66, relative to PS standards.

The yield for the synthesis of iPOP-$SC_5SO_2C_{12}$ was 90%. ^{1}H NMR (600 MHz, $CDCl_3$), δ (ppm) = 3.74 – 3.51 (m, ,-OC*H*$_2$C*H*O-, 3H), 3.01 – 2.91 (m, -CH$_2$C*H*$_2$SO$_2$C*H*$_2$CH$_2$-, 4H), 2.79 – 2.53 (m, -CHC*H*$_2$SC*H*$_2$CH$_2$-, 4H), 1.90 – 1.77 (m, ,-C*H*$_2$CH$_2$SO$_2$CH$_2$C*H*$_2$-, 4H), 1.69 – 1.50 (m, -CHCH$_2$SCH$_2$*CH*$_2$C*H*$_2$-, 4H), 1.48 – 1.19 (m, -CH$_2$(C*H*$_2$)$_9$CH$_3$, 18H), 0.88 (t, -C*H*$_3$, 3H). ^{13}C NMR (151 MHz, $CDCl_3$), δ (ppm) = 79.36, 71.14, 53.30, 52.41, 38.55, 33.93, 32.69, 31.84, 29.56, 29.50, 29.30, 29.28, 29.17, 29.11, 28.52, 27.65, 22.62, 21.82, 21.42, 14.06. SEC results with chloroform as eluent: $M_{n,SEC}$ = 202 kDa and $Đ$ = 1.83, relative to PS standards.

Synthesis of atactic and isotactic polyethers with disulfonyl pendant groups

All atactic and isotactic polyethers with disulfonyl pendant groups, aPOP-$SO_2C_5SO_2C_8$, aPOP-$SO_2C_5SO_2C_{12}$, iPOP-$SO_2C_5SO_2C_8$, and iPOP-$SO_2C_5SO_2C_{12}$ (Scheme 1), were synthesized from the corresponding polyethers with *n*-alkylsulfonylpentyl-thioether side chains using the same procedure. The following example shows the synthesis of aPOP-$SO_2C_5SO_2C_8$. *m*-CPBA (0.438 g, 1.78 mmol) and aPOP-$SC_5SO_2C_8$ (0.159 g, 0.47 mmol) were dissolved in chloroform (15 mL) in a 50 mL flask and stirred with a magnetic stir bar at room temperature for 3 h. The mixture was poured into a 150 mL separatory funnel and washed with 1 M NaOH (2 × 50 mL).

The organic layer was retrieved and dried with anhydrous sodium sulfate. After the removal of sodium sulfate and the solvent, the polymer was dried in a vacuum oven at 65 °C, yielding an opaque, brittle solid (0.156 g, 55% yield). ^{1}H NMR (500 MHz, $CDCl_3$), δ (ppm) = 4.22 – 3.59 (m, -OCH_2CHO-, 3H), 3.49 – 2.80 (m, -CHCH_2SO$_2$CH_2-, -CH_2SO$_2$CH_2(CH$_2$)$_6$CH$_3$, 8H), 1.96 – 1.73 (m, -CHCH$_2$SO$_2$CH$_2$CH_2CH$_2$CH_2CH$_2$SO$_2$ CH$_2$CH_2(CH$_2$)$_5$CH$_3$, 6H), 1.72 – 1.55 (m, -SO$_2$(CH$_2$)$_2$CH_2(CH$_2$)$_2$SO$_2$-, 2H), 1.51 – 1.20 (m, -(CH_2)$_5$CH$_3$, 10H), 0.88 (t, -CH_3, 3H). SEC results with chloroform as eluent: $M_{n,SEC}$ = 32.8 kDa and $Đ$ = 2.05, relative to PS standards.

The yield for the synthesis of aPOP-SO$_2$C$_5$SO$_2$C$_{12}$ was 93%. ^{1}H NMR (600 MHz, $CDCl_3$), δ (ppm) = 4.17 – 3.61 (m, -OCH_2CH- *3H*), 3.47 – 2.85 (m, -CHCH_2SO$_2$CH_2-, -CH_2SO$_2$CH_2(CH$_2$)$_{10}$CH$_3$, 8H), 1.97 – 1.73 (m, ,-CHCH$_2$SO$_2$CH$_2$CH_2CH$_2$CH_2CH$_2$SO$_2$CH$_2$CH_2-, 6H), 1.70 – 1.56 (m, -SO$_2$(CH$_2$)$_2$CH_2(CH$_2$)$_2$SO$_2$-, 2H), 1.47 – 1.04 (m, -(CH_2)$_9$CH$_3$, 18H), 0.88 (t, -CH_3, 3H). SEC results with chloroform as eluent: $M_{n,SEC}$ = 15.6 kDa and $Đ$ = 1.73, relative to PS standards.

The yield for the synthesis of iPOP-SO$_2$C$_5$SO$_2$C$_8$ was 31%. ^{1}H NMR (500 MHz, $CDCl_3$), δ (ppm) = 4.14 – 3.65 (m, -OCH_2CH-, 3H), 3.45 – 2.87 (m, -CHCH_2SO$_2$CH_2-, -CH_2SO$_2$CH_2(CH$_2$)$_6$CH$_3$, 8H), 1.94 – 1.75 (m, -SO$_2$CH$_2$CH_2CH$_2$CH_2CH$_2$SO$_2$CH$_2$CH_2-, 6H), 1.68 – 1.59 (m, -SO$_2$(CH$_2$)$_2$CH_2(CH$_2$)$_2$SO$_2$-, 2H), 1.47 – 1.22 [m, -(CH_2)$_5$CH$_3$, 10H], 0.89 (t, -CH_3, 3H). SEC results with chloroform as eluent: $M_{n,SEC}$ = 24.9 kDa and $Đ$ = 2.12, relative to PS standards.

The yield for the synthesis of iPOP-SO$_2$C$_5$SO$_2$C$_{12}$ was 68%. ^{1}H NMR (600 MHz, $CDCl_3$), δ (ppm) = 4.17 – 3.60 (m, -OCH_2CH- 3H), 3.51 – 2.82 (m, -CHCH_2SO$_2$CH_2-, -CH_2SO$_2$CH_2(CH$_2$)$_{10}$CH$_3$, 8H), 1.92 – 1.74 (m, -CHCH$_2$SO$_2$CH$_2$CH_2CH$_2$CH_2CH$_2$SO$_2$CH$_2$CH_2-, 6H), 1.69 – 1.57 [m, -SO$_2$(CH$_2$)$_2$CH_2(CH$_2$)$_2$SO$_2$-, 2H], 1.44 – 1.21 [m, -(CH_2)$_9$CH$_3$, 18H], 0.88 (t,

-C*H*$_3$, 3H). SEC results with chloroform as eluent: $M_{n,SEC}$ = 21.3 kDa and *Đ* = 1.69, relative to PS standards.

Results and discussion

Synthesis of isotactic and atactic polyethers with mono- and di-sulfonyl pendant groups

Isotactic and atactic POPs with mono-sulfonyl (i.e., *n*-alkylsulfonylpentylthioether) pendant groups were synthesized from aPECH and iPECH, respectively, via a substitution reaction, as illustrated in Scheme 1. iPECH was prepared by ring-opening polymerization of (*R*)-(-)-ECH using MMAO as catalyst, and we previously confirmed the isotacticity of the obtained iPECH by ^{13}C NMR spectroscopy. The substitution reactions of aPECH and iPECH with sodium 5-(*n*-octylsulfonyl)pentanethiolate and sodium 5-(*n*-dodecylsulfonyl)pentanethiolate, formed in-situ from 5-(*n*-octylsulfonyl)pentyl ethanethioate and 5-(*n*-dodecylsulfonyl)pentyl ethanethioate in the presence of sodium ethoxide, were carried out in DMAc at 100 °C for 48 h. After the isolation and purification, the obtained polymers were characterized by ^{1}H NMR spectroscopy to determine the degrees of substitution. Figures 1A and B show the ^{1}H NMR spectra of aPOP-$SC_5SO_2C_{12}$ and iPOP-$SC_5SO_2C_{12}$ in $CDCl_3$. The ^{1}H NMR spectra of aPOP-$SC_5SO_2C_8$ and iPOP-$SC_5SO_2C_8$ can be found in Figures S2A and S6A, respectively. A comparison of the peak integrals in the range of 3.75 – 3.53 ppm (-OC*H*$_2$C*H*- from the backbone) and 2.99 – 2.92 ppm (-CH$_2$C*H*$_2$SO$_2$C*H*$_2$CH$_2$- from the side chain) or 2.80 –2.51 ppm (-CHC*H*$_2$SC*H*$_2$CH$_2$- from the side chain) indicated that the substitution was essentially complete for all of the polymers.

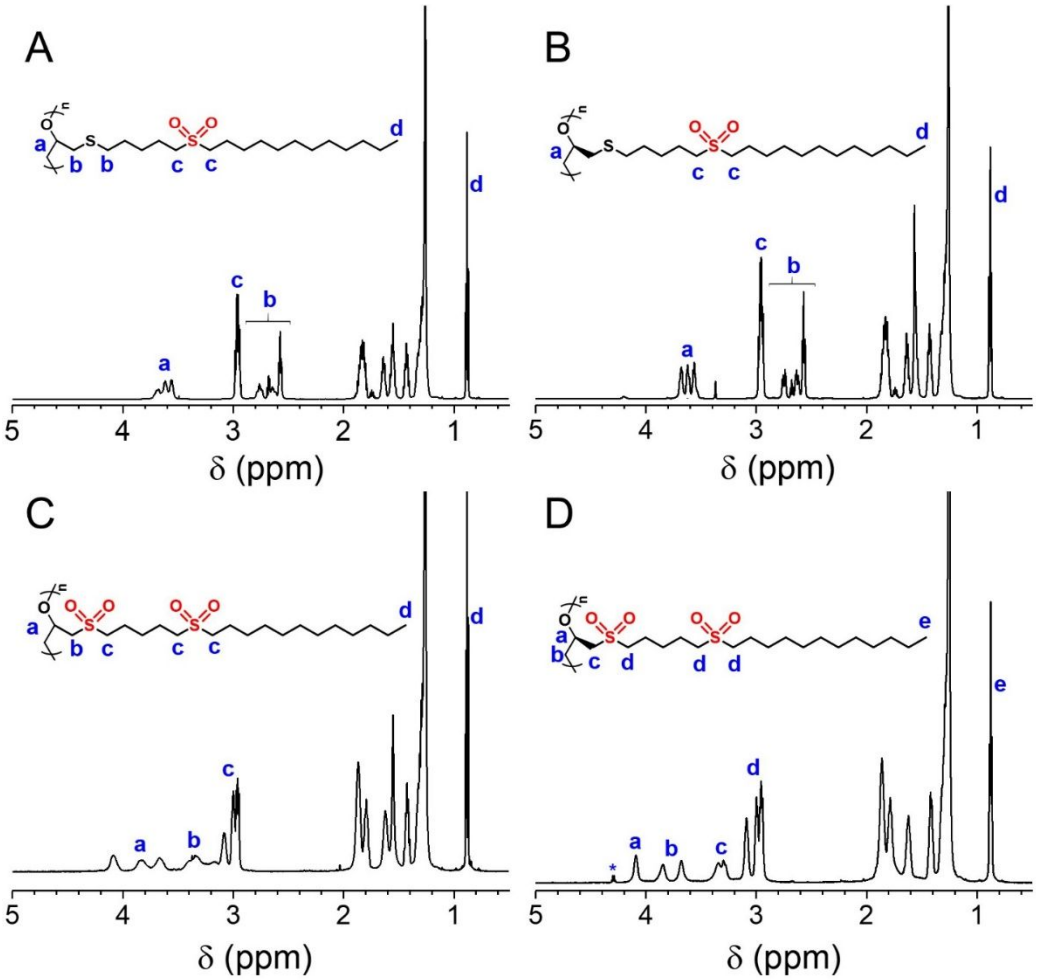

Figure 1. ^{1}H NMR spectra of (A) aPOP-$SC_5SO_2C_{12}$, (B) iPOP-$SC_5SO_2C_{12}$, (C) aPOP-$SO_2C_5SO_2C_{12}$, and (D) iPOP-$SO_2C_5SO_2C_{12}$ in $CDCl_3$. Peaks labeled with * are from impurities.

The polyethers with *n*-alkylsulfonylpentylthioether groups (i.e., POP-$SC_5SO_2C_8$ and POP-$SC_5SO_2C_{12}$) showed a reasonably good solubility in chloroform, allowing us to characterize the tacticity of these polymers by ^{13}C NMR spectroscopy, the optical activities of isotactic polymers by polarimetry, and the molecular weights and dispersities by SEC. Figure 2 shows the ^{13}C NMR spectra of aPOP-$SC_5SO_2C_{12}$ and iPOP-$SC_5SO_2C_{12}$ (those of aPOP-$SC_5SO_2C_8$ and iPOP-$SC_5SO_2C_8$ can be found in Figure S2B and S6B). While the backbone methylene (-*C*H_2-) carbon of the atactic polyethers manifested as multiple peaks in the range of 70 – 72 ppm, there was only a single peak at 71.1 ppm for both isotactic polyethers. These observations are

consistent with our previous results,[13] as well as the data reported by Brochu and Appleman.[39] Similarly, for the backbone methine carbon [-CH_2*C*H(CH_2S)O-], two peaks were observed at 79.20 and 79.34 for the two atactic polyethers, while the isotactic polymers (i.e., iPOP-$SC_5SO_2C_8$ and iPOP-$SC_5SO_2C_{12}$) exhibited only one peak at 79.33 ppm. Polarimetry measurements showed that atactic polymers did not exhibit an optical activity, with specific rotations of either zero or a negligible value. In contrast, iPOP-$SC_5SO_2C_8$ and iPOP-$SC_5SO_2C_{12}$ showed $[\alpha]_D^{20}$ values of -10.5 and -10.1°, respectively (Table 1). Note that the specific rotation of (*R*)-(-)-ECH monomer in methanol was -35.4° (with a concentration of ~10 mg/mL), which is much higher than those of the two isotactic polymers. This could be due to the different heteroatoms (Cl versus S) before and after the substitution and the different molar masses of the repeat units compared with (*R*)-(-)-ECH monomer (note that specific rotation [α] is calculated based on the concentration of ~10 mg/mL). If we assume that the contributions of Cl and $SC_5SO_2C_8$ or $SC_5SO_2C_{12}$ to the optical activity are identical, we can normalize the optical activities of iPOP-$SC_5SO_2C_8$ and iPOP-$SC_5SO_2C_{12}$ against the monomer based on the molar masses of the repeat unit. Then, the [α] values were -38.1° and -42.8°, which were comparable to that of (*R*)-(-)-ECH. SEC analysis showed that the $M_{n,SEC}$ values were from 48 to 202 kDa with respect to PS standards and the dispersities were in the range of 1.8 to 3.0 (Figures S3, S5, S7, and S9). These characterization data are summarized in Table 1, along with the specific rotations of iPOP-$SC_5SO_2C_8$ and iPOP-$SC_5SO_2C_{12}$.

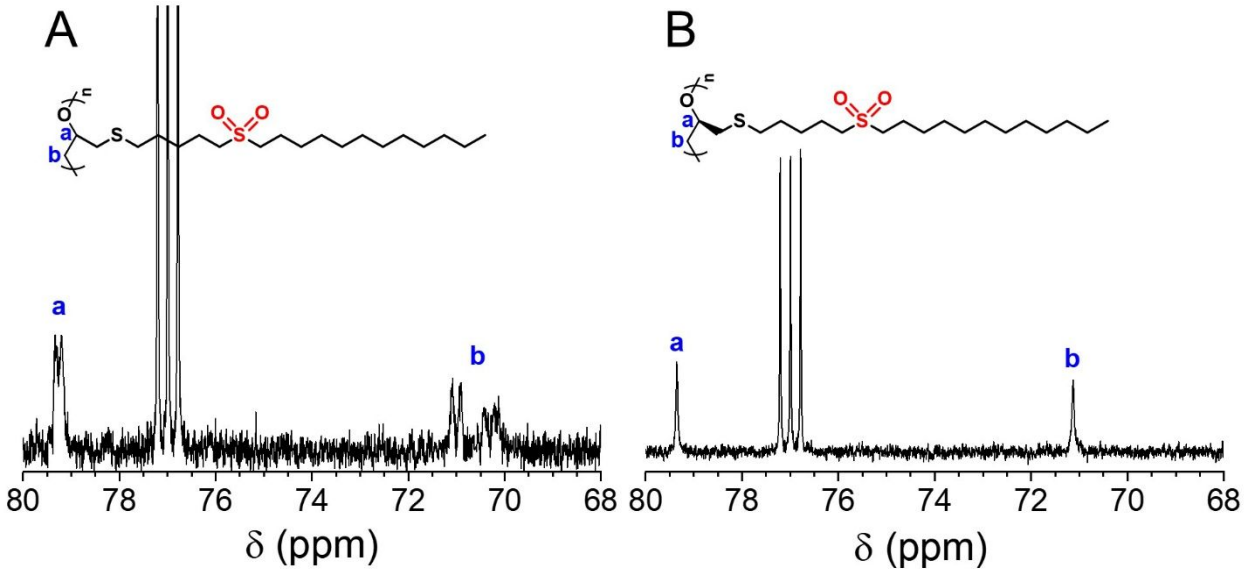

Figure 2. ^{13}C NMR spectra of (A) aPOP-$SC_5SO_2C_{12}$ and (B) iPOP-$SC_5SO_2C_{12}$ in $CDCl_3$.

Table 1. Characterization Data for Atactic and Isotactic Polyethers with Mono- and Di-sulfonyl Pendant Groups

Sample	$M_{n,SEC}$	$Đ$	$[\alpha]_D^{20}$	$T_{95\%}$
aPOP-$SC_5SO_2C_8$	129 kDa	3.04	-	327 °C
aPOP-$SO_2C_5SO_2C_8$	32.8 kDa	2.05	-	267 °C
iPOP-$SC_5SO_2C_8$	92.4 kDa	2.66	– 10.5°	328 °C
iPOP-$SO_2C_5SO_2C_8$	24.9 kDa	2.12	-	295 °C
aPOP-$SC_5SO_2C_{12}$	48.3 kDa	2.05	-	311 °C
aPOP-$SO_2C_5SO_2C_{12}$	15.6 kDa	1.73	-	333 °C
iPOP-$SC_5SO_2C_{12}$	202 kDa	1.83	– 10.1°	346 °C
iPOP-$SO_2C_5SO_2C_{12}$	21.3 kDa	1.69	-	299 °C

The polyethers with *n*-alkylsulfonylpentylthioether pendant groups were then oxidized by *m*-CPBA in chloroform at room temperature for 3 h to produce the polyethers with disulfonyl pendant groups (i.e., POP-$SO_2C_5SO_2C_8$ and POP-$SO_2C_5SO_2C_{12}$). ^1H NMR spectroscopy analysis showed that the peaks in the range of 2.50 – 2.80 ppm (-CH_2SCH_2-, the thioether linkage) completely disappeared for all four polyethers (Figure 1C and D for aPOP-$SO_2C_5SO_2C_{12}$ and iPOP-$SO_2C_5SO_2C_{12}$; Figure S10 shows the NMR spectra of aPOP-$SO_2C_5SO_2C_8$ and iPOP-$SO_2C_5SO_2C_8$), indicating that the oxidation of the thioether groups was complete. The molecular weights of the disulfonylated polyethers were also characterized by

SEC using $CHCl_3$ as eluent (Figure S11), and the data are summarized in Table 1. Compared with the $M_{n,SEC}$ for the thioether precursor polymers, the molecular weights decreased significantly for the disulfonylated polyethers. These results indicated that *m*-CPBA not only oxidized the thioether linkage in the side chains, but also randomly cleaved the polyether main chain. Nevertheless, the $M_{n,SEC}$ values for the resulting disulfonyl polyethers were high enough to be considered as polymers, not oligomers.

The thermal stability of atactic and isotactic polyethers with mono- and di-sulfonyl side chains was studied by TGA in a dry N_2 atmosphere at a heating rate of 20 °C/min, and the results are shown in Figure S12. The 5% weight loss temperatures ($T_{95\%}$) for the polyethers with *n*-alkylsulfonylthioether pendant groups are summarized in Table 1. The $T_{95\%}$ values for these polyethers were in the range of 310 – 345 °C, with those for the isotactic polymers being slightly higher. For the polyethers with disulfonyl pendant groups, the $T_{95\%}$ values were in the range of 267 – 332 °C, lower than those of the corresponding polyethers with *n*-alkylsulfonylthioether side chains (except for aPOP-$SO_2C_5SO_2C_{12}$). Due to the strong electron-withdrawing ability of the sulfonyl group, alkylsulfonyl compounds have been reported to be prone to β-H elimination, especially under the attack of basic impurities.[40] The different $T_{95\%}$ values of the disulfonyl polyethers may be related to the different amounts of impurities in the samples.

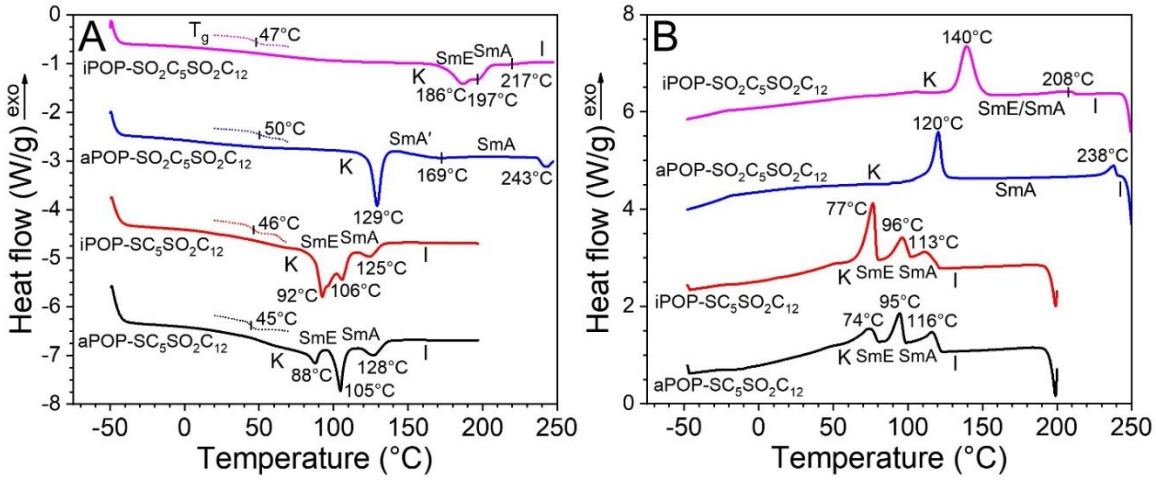

Figure 3. (A) Second heating DSC curves for atactic and isotactic POP-$SC_5SO_2C_{12}$ and POP-$SO_2C_5SO_2C_{12}$. (B) Second cooling DSC curves for atactic and isotactic POP-$SC_5SO_2C_{12}$ and POP-$SO_2C_5SO_2C_{12}$. The dotted lines in (A) show the T_g values during the first heating cycle. The heating and cooling rates are 20 °C/min.

Table 2. Peak Phase Transition Temperatures (above the arrow) and Heats of Transition (kJ/mol, below the arrow) [a] for atactic and isotactic POP-$SC_5SO_2C_{12}$ and POP-$SO_2C_5SO_2C_{12}$

Sample	Second Heating	Second Cooling
aPOP-$SC_5SO_2C_{12}$	K $\xrightarrow[5.5]{88°C}$ SmE $\xrightarrow[8.6]{105°C}$ SmA $\xrightarrow[4.8]{128°C}$ I	I $\xrightarrow[4.2]{116°C}$ SmA $\xrightarrow[4.3]{95°C}$ SmE $\xrightarrow[3.1]{74°C}$ K
iPOP-$SC_5SO_2C_{12}$	K $\xrightarrow[12.6]{92°C}$ SmE $\xrightarrow[6.6]{106°C}$ SmA $\xrightarrow[4.1]{125°C}$ I	I $\xrightarrow[2.7]{113°C}$ SmA $\xrightarrow[5.5]{96°C}$ SmE $\xrightarrow[10.6]{77°C}$ K
aPOP-$SO_2C_5SO_2C_{12}$	K $\xrightarrow[10.0]{129°C}$ SmA' $\xrightarrow[3.7]{169°C}$ SmA $\xrightarrow[2.1]{243°C}$ I	I $\xrightarrow[1.6]{238°C}$ SmA $\xrightarrow[9.1]{120°C}$ K
iPOP-$SO_2C_5SO_2C_{12}$	K $\xrightarrow[11.5]{186°C}$ SmE $\xrightarrow[1.2]{197°C}$ SmA $\xrightarrow[1.2]{217°C}$ I	I $\xrightarrow[1.3]{208°C}$ SmE/SmA $\xrightarrow[13.8]{140°C}$ K

[a] Heats of transition are obtained by peak deconvolution using Gaussian function.

Self-assembly of atactic and isotactic POP-$SC_5SO_2C_{12}$ and POP-$SO_2C_5SO_2C_{12}$

As shown in our previous report,[13] strong dipole-dipole interactions in comb-like polymers can induce liquid crystalline self-assembly even without any traditional mesogen groups. Here, we investigated the effects of main-chain chirality and chiral center-to-dipole distance on the self-assembly of atactic and isotactic mesogen-free polyethers with one and two sulfonyl groups in the side chains. DSC was first used to study the phase transitions in these strongly interacting comb-like polyethers. Figure 3 shows the second heating and second cooling DSC curves of

atactic and isotactic POP-$SC_5SO_2C_{12}$ and POP-$SO_2C_5SO_2C_{12}$. During the first heating, T_g was found in the range of 45-50 °C for all of the four polymers. During the second heating cycle, however, the T_g became less obvious. This is likely because the solution-precipitated samples had a lower crystallinity than those crystallized from the melt during DSC cooling, which made it possible for the polymers to exhibit clearer glass transitions. For both aPOP-$SC_5SO_2C_{12}$ and iPOP-$SC_5SO_2C_{12}$, three endothermic peaks were observed in a similar temperature range in the second heating and cooling cycle. The similar thermal behaviors for both atactic and isotactic POP-$SC_5SO_2C_{12}$ samples suggested that the main-chain chiral center had little effect on the self-assembly behavior when the sulfonyl dipole in the side chain was far (i.e., 7-atom) away from the chiral center. After the oxidation of the thioether groups with *m*-CPBA, both aPOP-$SO_2C_5SO_2C_{12}$ and iPOP-$SO_2C_5SO_2C_{12}$ exhibited increased phase transition temperatures. The thermal behavior of the isotactic disulfonyl sample appeared to be quite different from that of the atactic counterpart, indicating that the main-chain chiral center had a significant influence on the self-assembly behavior when a sulfonyl dipole was closer to the chiral center (i.e., separated by one CH_2 group). These phase transition temperatures and heats (summarized in Table 2) were used for subsequent PLM and XRD studies.

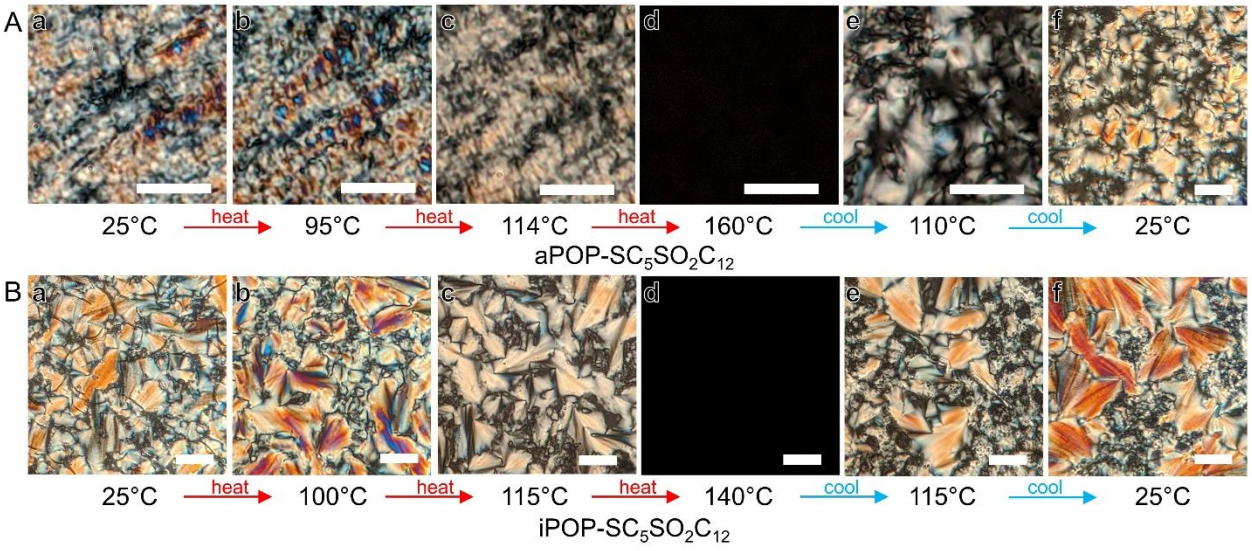

Figure 4. PLM images of (A) aPOPSC$_5$SO$_2$C$_{12}$ and (B) iPOPSC$_5$SO$_2$C$_{12}$ during the heating and cooling cycle. The scale bars are 20 μm.

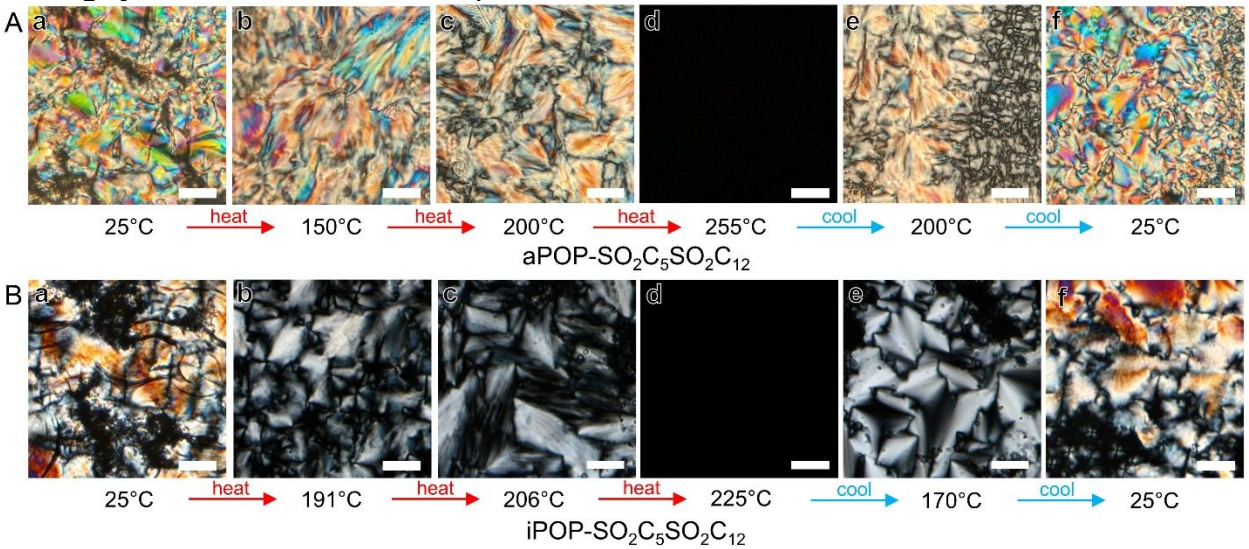

Figure 5. PLM images of (A) aPOPSO$_2$C$_5$SO$_2$C$_{12}$ and (B) iPOPSO$_2$C$_5$SO$_2$C$_{12}$ during the heating and cooling cycles. The scale bars are 20 μm.

Figures 4 and 5 show the PLM images for the POP-SC$_5$SO$_2$C$_{12}$ and POP-SO$_2$C$_5$SO$_2$C$_{12}$ samples, respectively. All samples showed obvious fan-shaped textures during the heating and cooling cycle, indicating that they all went through SmA type mesophases. Meanwhile, they exhibited no birefringence at temperatures above their corresponding T_i.

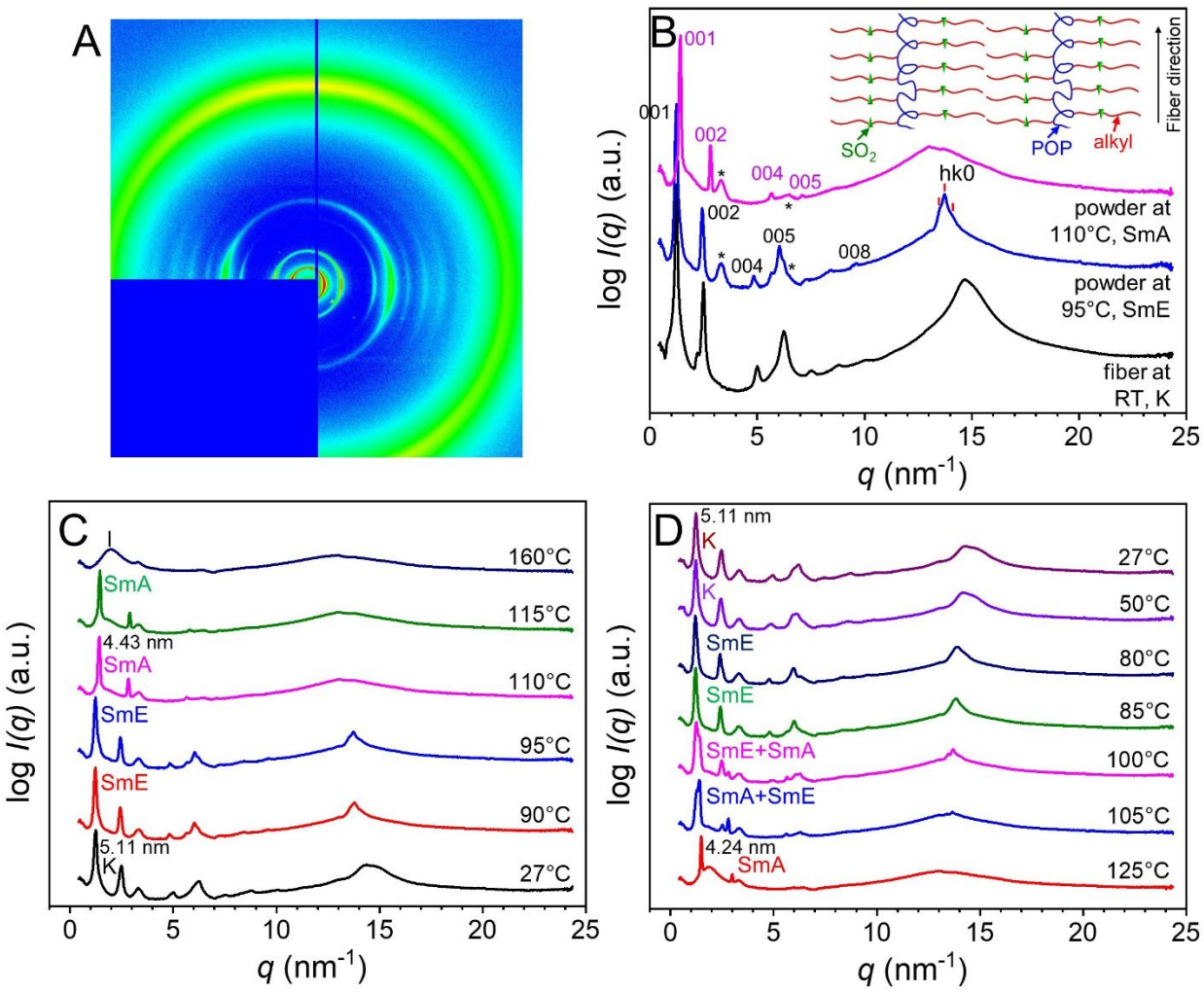

Figure 6. (A) 2D XRD pattern for the aPOP-$SC_5SO_2C_{12}$ fiber at room temperature. The fiber direction is vertical. (B) 1D XRD profiles for the aPOP-$SC_5SO_2C_{12}$ fiber at room temperature and the powder at 95 and 110 °C. The inset shows the schematic double layer structure. The bottom panel shows the 1D XRD profiles for the aPOP-$SC_5SO_2C_{12}$ powder during (C) heating and (D) cooling processes. Peaks labeled with * in B were from the Kapton window, and they are not labeled in C and D.

XRD was used to understand the mesophase structures of these samples. Results for aPOP-$SC_5SO_2C_{12}$ are shown in Figure 6. The fiber XRD pattern at room temperature in Figure 6A is consistent with the layered crystalline (K) structure in the comb-like polymer, as we reported before.[13] From the WAXD profiles at 27 °C (Figures 6C,D), multiple (hk0) reflections could be discerned for the K phase. In addition, the heats of fusion were also relatively large (see Table 2). All the evidence suggested the crystalline structure as the most stable phase. In

the fiber, the main chains supposedly are in the drawing (vertical) direction, and the side chains are perpendicular to the main chains. As a result, the side-chain lamellar crystals are parallel to the fiber direction. Indeed, well-ordered lamellar scattering [i.e., (00*l*) reflections] was seen in the horizontal direction with the *q* ratios being 1:2:4:5:6:7:8 (note that the 3rd order reflection was either very weak or extinct). The lamellar spacing was 5.11 nm, consistent with the double layer structure of the side chains having an all trans conformation (as reported before for the polyethers with *n*-alkylsulfonyl side chains,[13] the main chain was about 0.836 nm thick, and the length per CH_2/SO_2 was 0.118 nm); see the inset of Figure 6B. The (hk0) reflections in the wide-angle region concentrated on the vertical direction (Figure 6A). Given too few reflections in the fiber pattern, it is not possible to unambiguously determine the crystalline structure for the sample.

After heating to 95 °C, which was above the first endothermic peak at 88 °C but below the second endothermic peak at 105 °C (Figure 3A), the powder sample kept the double layer structure with the same layer spacing of 5.11 nm (Figure 6B, C, and D). This excluded chain-tilted structures. Note that three wide-angle (hk0) reflections became obvious and shifted to lower *q* values (Figure 6B). This excluded the hexatic B and smectic B (SmB) structures. Given these features, this structure was assigned as the smectic E (SmE) phase. From the point of view of unit cell structures, the K and the SmE phases have the same symmetry. However, a K phase has a long-range order (at least in one direction) whereas a SmE phase only has a quasi-long range order. This is often reflected from DSC heating and cooling curves. The K phase has a large energy barrier for nucleation and thus shows a large supercooling in DSC heating and cooling curves. However, the SmE phase has a small barrier for nucleation; therefore, no supercooling is often observed. When heating to 110 °C, which was between the second

endothermic peak (105 °C) and the third endothermic peak temperature (128 °C), the (001) reflection slightly shifted to a higher q value with a smaller double layer spacing of 4.43 nm (Figure 6B). The relatively sharp (hk0) reflections in the SmE phase disappeared and the wide-angle scattering became a single broad halo with its center further shifting to lower q (d = 0.47 nm). Given the lowest heat of fusion (Table 2), this phase could be determined as the smectic A (SmA) structure.

Figures 6C and D show 1D XRD profiles for the powder sample during heating and cooling processes, respectively. Reversible K↔SmE↔SmA phase transitions were observed, consistent with the DSC study in Figure 3. At 160 °C, the isotropic (I) phase with two amorphous halos at 1.98 (3.2 nm) and 13.08 nm^{-1} (0.48 nm) were observed, which originated from the density fluctuation-induced disordered structure[41, 42] and the average inter-side chain distance, respectively.

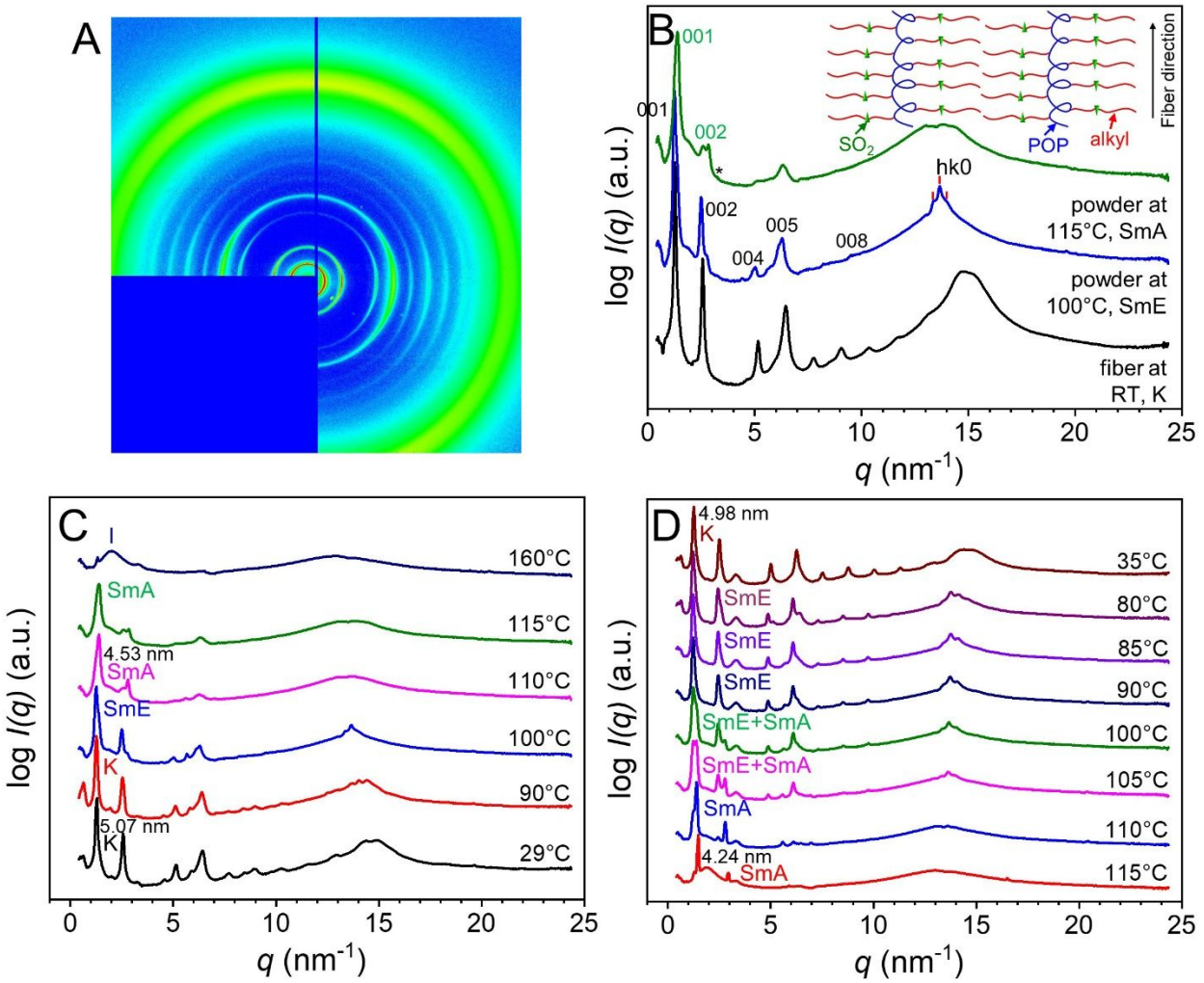

Figure 7. (A) 2D XRD pattern for the iPOP-$SC_5SO_2C_{12}$ fiber. The fiber direction is vertical. (B) 1D XRD profiles for the iPOP-$SC_5SO_2C_{12}$ fiber at room temperature and the powder at 100 and 115 °C. The inset shows the schematic double layer structure. The bottom panel shows the 1D XRD profiles for the iPOP-$SC_5SO_2C_{12}$ powder during (C) heating and (D) cooling processes. Peaks labeled with * in B were from the Kapton window, and they are not labeled in C and D.

For iPOP-$SC_5SO_2C_{12}$, a similar structure and phase transition behavior was observed. From the fiber XRD pattern in Figure 7A, a layered crystalline structure was observed with the *q* ratios being 1:2:4:5:6:7:8:9 (again, the 3rd order reflection is either very weak or distinct). The lamellar spacing was 5.07 nm, again consistent with the double layer structure with all trans side chains (see the inset of Figure 7B). The isotactic sample exhibited a SmE phase at 100 °C (lamellar spacing: 5.08 nm) and a SmA [i.e., chiral SmA (SmA*)] phase at 110 and 115 °C

(lamellar spacing: 4.53 nm); see Figure 7B. Upon heating and cooling, reversible K↔SmE↔SmA phase transitions were observed (Figures 7C and D). Comparing the structures and phase transitions, the differences between aPOP-$SC_5SO_2C_{12}$ and iPOP-$SC_5SO_2C_{12}$ are quite small. Therefore, we can conclude that the chiral center on the main chain has little influence on the structure and transitions when the SO_2 dipole is far away from the chiral center, which provides a valuable guide to us in the future design of ferroelectric liquid crystalline polymers.

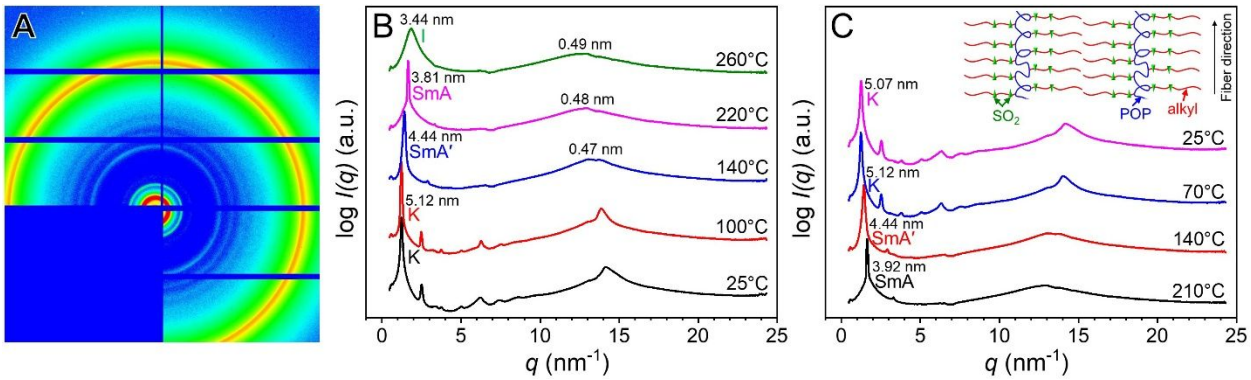

Figure 8. (A) 2D XRD pattern for the aPOP-$SO_2C_5SO_2C_{12}$ powder at room temperature. (B) and (C) show 1D XRD profiles for the powder sample during the heating and cooling cycles, respectively. The inset shows the schematic double layer structure.

After oxidizing the thioether to the sulfonyl group, the self-assembly behavior changed substantially as a result of additional strong dipole-dipole interactions among the sulfonyl groups adjacent to the main chain. Figure 8A shows the 2D XRD powder pattern of aPOP-$SO_2C_5SO_2C_{12}$ at room temperature, revealing a layered crystalline structure. We note here that oriented fibers were very difficult to obtain for these disulfonyl samples, possibly due to the highly crystalline structure. The lamellar spacing was 5.12 nm, again consistent with the double layer structure with the side chains perpendicular to the main chain (see the inset of Figure 8C). Upon heating, this K phase was stable up to 129 °C (Figure 3A), above which the sharp wide-angle peak around 13.88 nm^{-1} disappeared, and the sample transformed sequentially into two SmA phases with a slightly different layer spacing; 4.44 nm for the SmA′ in the temperature

range of 129 to 169 °C (Figure 3A) and 3.81 nm in the range of 169 – 243 °C for SmA. A similar SmA' phase with partial interdigitation was also reported before for other atactic samples.[34] Above 243 °C, the sample entered the I phase with two amorphous halos at 1.86 (3.44 nm) and 12.70 nm^{-1} (0.49 nm), respectively (Figure 8B), slightly larger than those of aPOP-$SC_5SO_2C_{12}$ in the I phase at 160 °C (3.2 nm and 0.48 nm, respectively, Figure 6C). Upon cooling, reverse phase transitions were seen as shown in Figure 8C. Compared with aPOP-$SC_5SO_2C_{12}$ having one sulfonyl group far away from the main chain, aPOP-$SO_2C_5SO_2C_{12}$ has much higher T_m and T_i. This can be explained by the additional dipole-dipole interaction and also smaller entropy change during the phase transitions. Currently, it is not clear why the SmE phase was not observed for this sample.

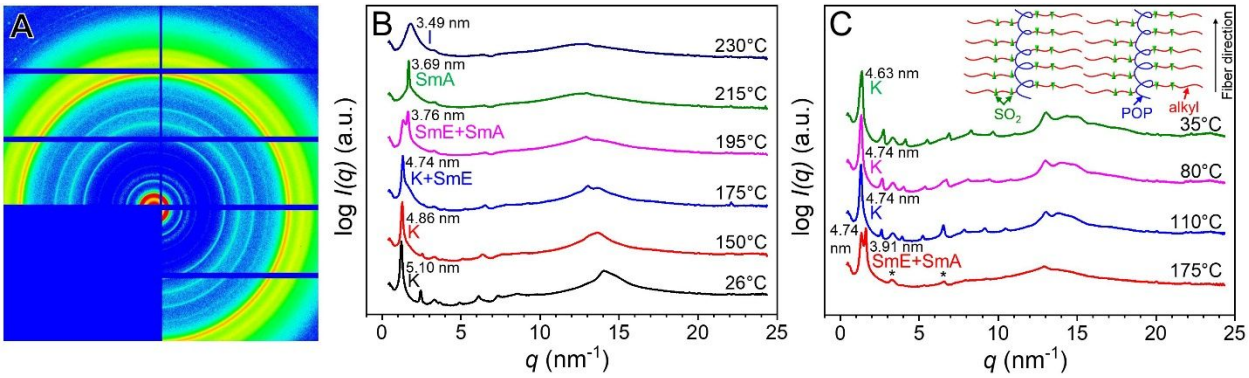

Figure 9. (A) 2D XRD pattern for the iPOP-$SO_2C_5SO_2C_{12}$ powder at room temperature. (B) and (C) show 1D XRD profiles for the iPOP-$SO_2C_5SO_2C_{12}$ powder during the heating and cooling processes, respectively. The inset shows the schematic double layer structure.

For iPOP-$SO_2C_5SO_2C_{12}$, the T_m was pushed to even higher temperatures (186 °C) due to the regular packing of the side chains and strong dipole-dipole interactions (see Figure 3A). At room temperature, the layered crystalline structure was again observed (Figure 9A). The lamellar spacing was 5.10 nm, indicating the double layer structure (see the inset of Figure 9C). Upon heating to 175 °C, part of the crystals melted into the SmE phase with multiple (hk0) peaks

in the wide-angle region (Figure 9B). Further heating to 195-215 °C, a SmA (or SmA*) phase appeared with a layer spacing of 3.69 nm. Finally at 230 °C, the I phase was obtained. Because of high T_m, the T_m to T_i range was quite small for iPOP-$SO_2C_5SO_2C_{12}$. The T_i of iPOP-$SO_2C_5SO_2C_{12}$ was in fact lower than the T_i of aPOP-$SO_2C_5SO_2C_{12}$ by more than 20 °C. For the SmA phase before the I phase, iPOP-$SO_2C_5SO_2C_{12}$ might have a lower entropy compared to aPOP-$SO_2C_5SO_2C_{12}$. If we assume that their I phases had a similar entropy, then a smaller entropy change will be expected for the isotropization of aPOP-$SO_2C_5SO_2C_{12}$. As a result, aPOP-$SO_2C_5SO_2C_{12}$ exhibited a higher T_i than iPOP-$SO_2C_5SO_2C_{12}$. Upon cooling, the reverse I→SmA→SmE→K transitions were observed (Figure 9C).

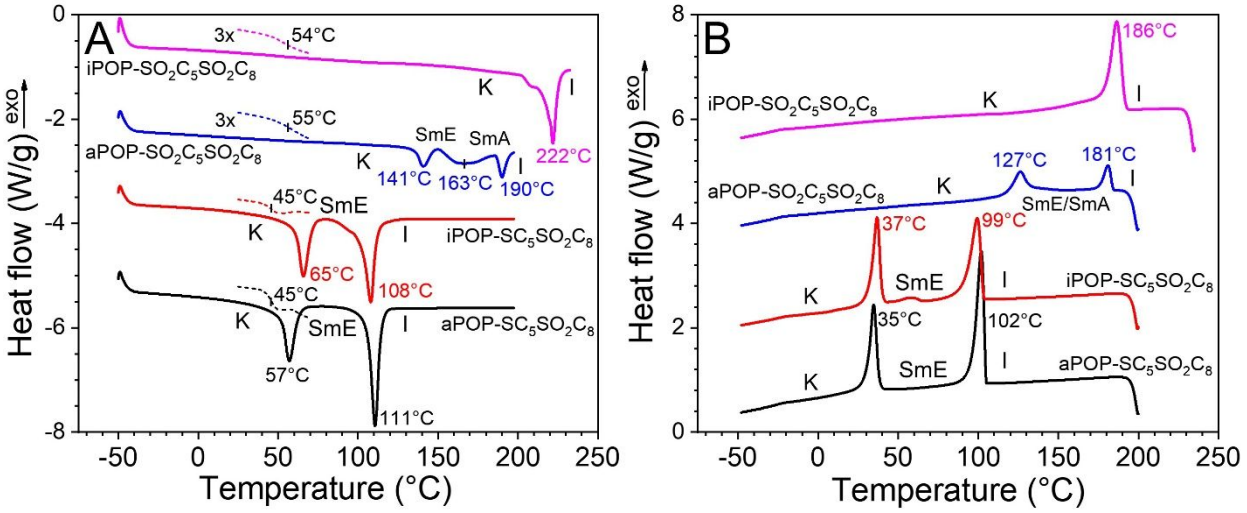

Figure 10. (A) DSC second heating curves for atactic and isotactic POP-$SC_5SO_2C_8$ and POP-$SO_2C_5SO_2C_8$. (B) DSC second cooling curves for atactic and isotactic POP-$SC_5SO_2C_8$ and POP-$SO_2C_5SO_2C_8$. K: crystal, SmE: smectic E, SmA: smectic A, and I: isotropic. T_g values are determined from the first heating (thin dotted lines in the insets).

Table 3. Peak Phase Transition Temperatures (above the arrow) and Heats of Transition (kJ/mol, below the arrow) [a] for atactic and isotactic POP-$SC_5SO_2C_8$ and POP-$SO_2C_5SO_2C_8$

Sample	Second Heating	Second Cooling
aPOP-$SC_5SO_2C_8$	K $\xrightarrow[9.1]{57°C}$ SmE $\xrightarrow[14.5]{111°C}$ I	I $\xrightarrow[15.0]{102°C}$ SmE $\xrightarrow[9.6]{35°C}$ K
iPOP-$SC_5SO_2C_8$	K $\xrightarrow[9.6]{65°C}$ SmE $\xrightarrow[14.0]{108°C}$ I	I $\xrightarrow[12.5]{99°C}$ SmE $\xrightarrow[9.7]{37°C}$ K

aPOP-$SO_2C_5SO_2C_8$	K $\xrightarrow[2.9]{141^\circ C}$ SmE $\xrightarrow[7.7]{163^\circ C}$ SmA $\xrightarrow[2.7]{190^\circ C}$ I	I $\xrightarrow[2.8]{181^\circ C}$ SmE/SmA $\xrightarrow[6.9]{127^\circ C}$ K
iPOP-$SO_2C_5SO_2C_8$	K $\xrightarrow[16.0]{222^\circ C}$ I	I $\xrightarrow[14.4]{186^\circ C}$ K

[a] Heats of transition are obtained in units of kJ/mol by peak deconvolution using Gaussian function.

Effect of *n*-alkyl tail length on self-assembly of atactic and isotactic POP-$SC_5SO_2C_8$ and POP-$SO_2C_5SO_2C_8$

From the above study, we understand that chirality is effective in changing the liquid crystalline self-assembly behavior, when the sulfonyl dipole is close to the chiral center [i.e., stronger chiral center-dipole interaction (or chiral center-induced stronger dipole-dipole interaction)]. How will the *n*-alkyl tail length affect the self-assembly of atactic and isotactic sulfonylated polyethers? To answer this question, we reduced the side-chain alkyl tail length from C_{12} to C_8. Figures 10A and B show the second heating and second cooling DSC curves for atactic and isotactic POP-$SC_5SO_2C_8$ and POP-$SO_2C_5SO_2C_8$, respectively. The T_m, and T_i values and the corresponding heats of fusion are summarized in Table 3. From the PLM and XRD studies (see Section III in the Supporting Information), different mesophases were identified. For example, atactic and isotactic POP-$SC_5SO_2C_8$ exhibited K, SmE, and I phases with increasing temperature. The difference in structure and phase transitions between these two samples were small, corroborating our observations from aPOP-$SC_5SO_2C_{12}$ and iPOP-$SC_5SO_2C_{12}$ that the chiral center in the main chain had little effect on the liquid crystalline self-assembly when the sulfonyl dipole was far away. Compared with POP-$SC_5SO_2C_{12}$ samples, a notable difference is the absence of the SmA phase, which is likely because the shorter *n*-alkyl tail could not stabilize the SmA phase. In addition, the T_m and T_i values of atactic and isotactic POP-$SC_5SO_2C_8$ were lower than those of atactic and isotactic POP-$SC_5SO_2C_{12}$. These results suggested that the van der

Waals interaction among the relatively long alkyl tails should also play an important role in the self-assembly. A similar phenomenon was previously reported for atactic and isotactic POP-SO_2C_n, namely, T_m and T_i increased upon increasing the *n*-alkyl tail length.[13]

For aPOP-$SO_2C_5SO_2C_8$, the K→SmE→SmA→I phase transitions were observed upon heating (see structure identification in Section III in the Supporting Information). The T_m was higher whereas the T_i was lower than those for aPOP-$SO_2C_5SO_2C_{12}$. For iPOP-$SO_2C_5SO_2C_8$, only a high T_m around 222 °C was observed. From these results, it is likely that the strong dipole-dipole interaction among the disulfonyl groups overwhelmed the van der Waals interactions among the alkyl tails.

Conclusions

In this work, the effects of main-chain chirality (i.e., isotactic vs. atactic), chiral center-to-dipole distance, number of sulfonyl dipoles per side chain, and *n*-alkyl tail length on liquid crystalline self-assembly behavior of sulfonylated polyethers were investigated in our continued effort to seek for SmC* phases in mesogen-free comb-like polymers. The main findings are summarized below.

i) The main-chain chirality had little effect on the self-assembly of POP-$SC_5SO_2C_{12}$ and POP-$SC_5SO_2C_8$, because the sulfonyl dipole was far away from the chiral center (i.e., weak chiral center-dipole interaction). As a result, both atactic and isotactic polyethers exhibited the same phase transitions (K→SmE→SmA→I for POP-$SC_5SO_2C_{12}$ and K→SmE→I for POP-$SC_5SO_2C_8$) with similar transition temperatures.

ii) The alkyl tail length played an important role in the self-assembly of POP-$SC_5SO_2C_{12}$ and POP-$SC_5SO_2C_8$ due to the van der Waals interactions. Namely, the longer the alkyl tails, the

higher the phase transition temperatures. In addition, the longer *n*-alkyl tail (C_{12}) stabilized the SmA phase and no such mesophases were found in the POP-$SC_5SO_2C_8$ between the SmE and I phases.

iii) After the oxidation of the thioether to the second sulfonyl group, the adjacent chiral center in iPOP-$SO_2C_5SO_2C_{12}$ significantly changed the self-assembly behavior as compared to aPOP-$SO_2C_5SO_2C_{12}$, i.e., the crystal T_m and liquid crystalline transition temperatures were shifted to much higher temperatures. Meanwhile, the dipole-dipole interactions among the disulfonyl side chains were much stronger, overwhelming the van der Waals interactions among the alkyl tails. As a result, the alkyl tail length played a less significant role in the self-assembly of disulfonylated polyethers. For iPOP-$SC_5SO_2C_8$, the changes in self-assembly after the oxidation were even more dramatic, with no liquid crystalline phases observed but the direct melting of the K to the I phase, while aPOP-$SO_2C_5SO_2C_8$ exhibited reversible K→SmE→SmA→I phase transitions.

Although strongly interacting mono- or di-sulfonyl groups could induce liquid crystalline self-assembly (SmE and SmA) in these mesogen-free polyethers, the targeted SmC* phase was not realized in the polyethers with chiral centers in the main chain, regardless of whether there were one or two sulfonyl groups in each side chain. Note that the SmA phase in the isotactic polyethers should be chiral SmA, which has been reported to have a giant electroclinic property.[43] To achieve the SmC* phase, most studies choose to implement the chiral center in the side chains, in either the aliphatic spacer between the main chain and the dipole or the tail.[2] Meanwhile, it is important to keep the dipole close to the chiral center. Currently, we are implementing the chiral center in the side chains to induce the SmC* phase. The findings reported in this work not only enhance our understanding of the liquid crystalline self-assembly

behavior of polyethers with sulfonyl side chains, but also provide a valuable guide in the design of new mesogen-free chiral liquid crystalline polymers with ferroelectric behavior.

Conflicts of Interest

There are no conflicts of interest to declare.

Acknowledgements

This work is supported by the U.S. Department of Energy (DOE), Office of Science/Basic Energy Science, Materials Synthesis Program under the grant number DE-SC0018075. XRD experiments were performed with the help of Dr. Masafumi Fukuto at the 11-BM CMS beamline of NSLS-II, BNL, a U.S. DOE User Facility operated for the Office of Science by BNL under Contract DESC0012704.

Electronic Supplementary Information (ESI) available: Synthesis of starting materials, NMR, SEC, and TGA characterization of various mono- and di-sulfonylated polyethers, and PLM and XRD characterization of atactic and isotactic POP-$SC_5SO_2C_8$ and POP-$SO_2C_5SO_2C_8$. See DOI: xxxxxxxxxxxxxxxxx

References

1. S. Pirkl and M. Glogarova, in *Ferroelectrics - Physical Effects*, M. Lallart, Ed., InTech, 2011, Chapter 17, pp. 407-428.
2. G. Scherowsky, in *Ferroelectric Polymers: Chemistry, Physics, and Applications*, H. S. Nalwa, Ed., Marcel Dekker, Inc., New York, 1995, Chapter 10, pp. 435-537.
3. R. Zentel and M. Brehmer, *Adv. Mater.*, 1994, 6, 598-599.
4. M. Brehmer, R. Zentel, G. Wagenblast and K. Siemensmeyer, *Macromol. Chem. Phys.*, 1994, 195, 1891-1904.

5. S. Shilov, E. Gebhard, H. Skupin, R. Zentel and F. Kremer, *Macromolecules*, 1999, 32, 1570-1575.

6. F. Kremer, W. Lehmann, H. Skupin, C. Tolksdorf, E. Gebhard, R. Zentel, P. Kruger and M. Losche, *Nature*, 2001, 410, 447-450.

7. Y. Yu, T. Maeda, J. Mamiya and T. Ikeda, *Angew. Chem. Int. Ed.*, 2007, 46, 881-883.

8. C. Ohm, M. Brehmer and R. Zentel, *Adv. Mater.*, 2010, 22, 3366-3387.

9. H. Luo, C. Ma, X. Zhou, S. Chen and D. Zhang, *Macromolecules*, 2017, 50, 5132-5137.

10. S. M. Nakhmanson, M. B. Nardelli and J. Bernholc, *Phys. Rev. Lett.*, 2004, 92, 115504.

11. S. M. Nakhmanson, M. B. Nardelli and J. Bernholc, *Phys. Rev. B*, 2005, 72, 115210.

12. Y. C. Shu and K. Bhattacharya, *Philos. Mag. B*, 2001, 81, 2021-2054.

13. M.-Kwok, B. Seymour, R. Li, M. Litt, B. Zhao and L. Zhu, *Macromolecules*, 2019, 52, 3601-3611.

14. L. Zhu, *J. Phys. Chem. Lett.*, 2014, 5, 3677-3687.

15. P. K. Mukherjee, *Phys. Rep.*, 2015, 588, 1-54.

16. D. C. Bassett, *Principles of Polymer Morphology*, Cambridge University Press, Cambridge, U.K., 1981.

17. S. Rastogi, M. Newman and A. Keller, *Nature*, 1991, 353, 55-57.

18. T. Hattori, M. Hikosaka and H. Ohigashi, *Polymer*, 1996, 37, 85-91.

19. T. Hattori, T. Watanabe, S. Akama, M. Hikosaka and H. Ohigashi, *Polymer*, 1997, 38, 3505-3511.

20. T. Furukawa, *Adv. Colloid Interface Sci.*, 1997, 71-2, 183-208.

21. K. Tashiro and R. Tanaka, *Polymer*, 2006, 47, 5433-5444.

22. V. P. Shibaev, R. V. Talroze, F. I. Karakhanova and N. A. Plate, *J. Polym. Sci., Polym. Chem. Ed.*, 1979, 17, 1671-1684.

23. N. A. Plate and V. P. Shibaev, *Comb-Shaped Polymers and Liquid Crystals*, Springer, Boston, 1987.

24. S. M. Aharoni, *Macromolecules*, 1988, 21, 1941-1961.

25. T. H. Zhang, M. H. Litt and C. E. Rogers, *J. Polym. Sci., Part A: Polym. Chem.*, 1994, 32, 2809-2816.

26. T. H. Zhang, M. H. Litt and C. E. Rogers, *J. Polym. Sci., Part A: Polym. Chem.*, 1994, 32, 2291-2300.

27. T. H. Zhang, M. H. Litt and C. E. Rogers, *J. Polym. Sci., Part A: Polym. Chem.*, 1994, 32, 1351-1360.

28. T. H. Zhang, M. H. Litt and C. E. Rogers, *J. Polym. Sci., Part A: Polym. Chem.*, 1994, 32, 1531-1537.

29. J.-C. Lee and M. H. Litt, *J. Ind. Eng. Chem.*, 1999, 5, 155-159.

30. J.-C. Lee, M. H. Litt and C. E. Rogers, *Macromolecules*, 1997, 30, 3766-3774.

31. J.-C. Lee, M. H. Litt and C. E. Rogers, *Macromolecules*, 1998, 31, 2440-2446.

32. J.-C. Lee, K. Oh, H. B. Lee, Y. G. Kim, J. Y. Jho, S. Y. Kwak, S. Y. Park and B. L. Farmer, *Macromol. Rapid Commun.*, 2001, 22, 815-819.

33. S. Y. Park, B. L. Farmer and J.-C. Lee, *Polymer*, 2002, 43, 177-183.

34. J.-C. Lee, S. H. Han, S. H. Cha, S. Y. Park and B. L. Farmer, *Polymer*, 2003, 44, 7413-7425.

35. J. U. Kim and J.-C. Lee, *Macromol. Chem. Phys.*, 2005, 206, 951-960.

36. B. G. Kim, J. K. Moon, E. H. Sohn, J.-C. Lee and J. K. Yeo, *Macromol. Res.*, 2008, 16, 36-44.

37. B. G. Kim, J. S. Chung, E. H. Sohn, S. Y. Kwak and J.-C. Lee, *Macromolecules*, 2009, 42, 3333-3339.

38. S. T. Lagerwall, *Ferroelectric and Antiferroelectric Liquid Crystals*, Wiley-VCH, Weinheim, 1999.

39. S. Brochu and G. Ampleman, *Macromolecules*, 1996, 29, 5539-5545.

40. Y. L. Zhao, W. H. Jones, F. Monnat, F. Wudl and K. N. Houk, *Macromolecules*, 2005, 38, 10279-10285.

41. N. Sakamoto and T. Hashimoto, *Macromolecules*, 1995, 28, 6825-6834.

42. N. Sakamoto and T. Hashimoto, *Macromolecules*, 1998, 31, 3815-3823.

43. S. Nishiyama, Y. Ouchi, H. Takezoe and A. Fukuda, *Japn. J. Appl. Phys.* 1987, 26, L1787-L1789.

TABLE OF CONTENT GRAPHIC

AUTHOR NAMES

Caleb A. Bohannon, Man-Hin Kwok,* Ruipeng Li, Lei Zhu, Bin Zhao*

TITLE

Effects of tacticity and chiral center-to-dipole distance on mesogen-free liquid crystalline self-assembly of sulfonyl-containing comb-like polymers

TEXT

Mesogen-free comb-like polyethers bearing strongly interacting mono- and di-sulfonylated side chains exhibit well-defined liquid crystalline self-assembly.

GRAPHICAL ABSTRACT FIGURE